RSC Advances

ROYAL SOCIETY OF CHEMISTRY

www.rsc.org/advances

RSC Advances

RSCPublishing

ARTICLE

Visible-Light-Driven MWCNT@TiO_2 Core-shell Nanocomposites and the Roles of MWCNTs on the Surface Chemistry, Optical Properties and Reactivity in CO_2 Photoreduction

Cite this: DOI: 10.1039/x0xx00000x

Received 00th January 2012,
Accepted 00th January 2012

DOI: 10.1039/x0xx00000x

www.rsc.org/

Meei Mei Gui[a], Siang-Piao Chai[a,]*, Bo-Qing Xu[b], Abdul Rahman Mohamed[c]

Multi-walled carbon nanotube (MWCNT)@titanium dioxide (TiO_2) core-shell structures were synthesized through a simple coating approach in this work. Varying the ratio of TiO_2 to MWCNTs revealed the importance of MWCNT loading in controlling the uniformity of the core-shell structures and their photocatalytic performance. These core-shell nanocomposites possessed an excellent visible light absorption with the absorption edge extended into visible light range of 380-600nm with respect to the MWCNT loading. The inhibition of electron-hole pair recombination was found to be greater with the increase in the MWCNT loading, revealing that the presence of MWCNTs in the composites enhanced the electron transfer and reduced the electron-hole pair recombination rates. The MWCNT@TiO_2 core-shell nanocomposites exhibited promising photocatalytic activity in carbon dioxide reduction, giving the maximum methane formation of 1.10μmol/g-TiO_2 for 8h of reaction under visible light irradiation at atmospheric temperature and pressure.

1. Introduction

Increasing level of carbon dioxide (CO_2) in the atmosphere is the primary cause of global warming. Plenty efforts have been devoted to reduce CO_2 emissions. Among them, photoreduction of CO_2 with water has emerged to be one of the important alternatives to convert CO_2 into useful hydrocarbon compounds. CO_2 reduction through photocatalysis resembles natural photosynthesis, which has always been the most energy competent method for direct conversion of CO_2 into hydrocarbons. Visible-light-driven photocatalysis, being the extraordinary energy effectiveness route, is highly desired in order to fully harvest solar energy. However, the production of CO_2-free fuels by direct conversion of solar energy into chemical energy is still a challenge within the scientific community due to the relative low energy content of the visible light as compared to ultraviolet (UV) light.

Anatase titanium oxide (TiO_2) is commonly used for the photocatalytic processes due to its bandgap value of approximately 3.2eV[1] and its unique properties such as strong oxidizing power and long-term photostability.[2,3] However, TiO_2 has poor performance in visible light irradiated photoreaction as a result of its bandgap falls under the UV region. On the other hand, carbon nanotubes (CNTs) have successfully drawn extensive interests in recent years owing to their unique optical properties and excellent electron transfer ability. CNTs have been widely reported to stimulate the photocatalytic activity of anatase TiO_2 by electron charge transfer through the heterojunction of the CNTs and the TiO_2 surfaces.[4] CNTs play the role as electron storage which can store up to 1 electron per 32 carbon atoms during photoexcitation and release the electrons back to the surrounding medium when the electron concentration in its surrounding is low upon the photoreaction process.[5] CNTs are also the electron sinks that transfer the electrons away from the TiO_2 particles after photoexcitation, leaving behind holes on the surface of the TiO_2. These electrons can trigger the photoreaction by formation of very reactive radicals such as superoxide radical ions ($O_2^{\bullet -}$) and hydroxyl radicals ($HO^{\bullet}$).[6,7] In addition, CNTs also possess high mechanical strength, good chemical stability and large specific surface area, which are the important criteria for a superior catalyst support.[8]

Extensive efforts have been devoted to the modification of TiO_2 with the addition of CNTs. The CNTs-TiO_2 hybrid composites are commonly synthesized using sol-gel,[9-13] chemical vapor deposition,[14] functionalization with titanium precursor,[15] and solvothermal method.[16] Hydrothermal has been widely used for the synthesis of CNTs-TiO_2 composites due to the simplicity of the process. However, it is challenging to obtain CNTs@TiO_2 core-shell structures due to the fact that the TiO_2 formation rate is hard to control. The dispersion of the TiO_2 in the structure could affect the role of CNTs as electron sink and/or electron

storage in a photocatalytic reaction. It is known that the electrons will transfer between the TiO_2 and the CNTs through the heterojunctions where these two composites are contacted.[17] Well-dispersed TiO_2 particles on the CNT could seize optimum electron charge transfer and maximize the inhibition of the electron-hole pair recombination, thus improving the overall photocatalytic activity.

In this work, core-shell nanocomposites comprising of multi-walled carbon nanotubes (MWCNTs) and TiO_2 were synthesized. The effects of the MWCNT loading on the optical properties and photoreactivity of the composites were investigated. The characteristics of the MWCNT@TiO_2 and their application in CO_2 photoreduction reaction were also studied. The CO_2 photoreduction reaction was carried out in a custom-fabricated reactor with continuous CO_2 flow. Water was used as the sacrificial agent and low power energy saving light bulb as the visible light source.

2. Materials and Methodology

2.1 Synthesis of MWCNT@TiO_2 core-shell structure

The MWCNT@TiO_2 core-shell structure was synthesized in a two-step coating approach as reported in our previous study.[18] In the first step, the MWCNTs were acid-treated to remove metal catalysts and to introduce surface carboxyl groups on the MWCNTs. The introduction of surface carboxyl groups was intended to bring the hydrophilic behaviour of the MWCNTs which would ease the subsequent TiO_2 coating process. In the second step, TiO_2 (shell) was coated on MWCNT (core) using titanium butoxide (TBOT, Sigma Aldrich, 97%).[18] The ratio of TiO_2 to MWCNTs (g/g) was varied as listed in Table 1.

Table 1: Sample labels for the composites with different TiO_2 to MWCNTs ratios (g/g).

Sample name	Ratio of TiO_2: MWCNTs (g/g)
TiOCNT1	1: 0.04
TiOCNT2	1: 0.08
TiOCNT3	1: 0.16
TiOCNT4	1: 0.24
TiOCNT5	1: 0.32
TiOCNT6	1: 0.40

2.2 Materials characterization

There are generally few important characteristics that are in strong interest for developing a photocatalyst, such as light absorption, surface morphology, crystal phase and surface chemistry. Light absorption performance of the nanocomposites was analysed by UV-vis diffuse reflectance spectroscopy (Agilent, Cary 100) with the wavelength of 200-800nm, covering UV and visible range. Field emission-scanning electron microscopy (FE-SEM, Hitachi SU8010) was carried out to investigate the surface morphology of the developed nanocomposites. The lattice structures were studied with high-resolution transmission electron microscopy (HRTEM, JEM2100) operated at 200kV. Raman spectroscopy (Renishaw inVia Raman microscope) was employed to study the effect of MWCNT loading on the surface chemistry and photoluminescence (PL) analysis (Renishaw inVia) was conducted to study the electron-hole pair recombination rate of the MWCNT@TiO_2 using Ar ion laser with a wavelength of 325nm. On the other hand, X-ray diffraction (XRD) was employed to analyze the crystal structure of the TiO_2 obtained. Crystallite sizes of the TiO_2 nanoparticles were estimated at FWHM (full-width at half maximum) based on the Scherrer's equation:

$$B = \frac{K\lambda}{\beta \cos\theta} \quad \text{(Eq. 1)}$$

Where; B is the crystallite size of the XRD maximum peak (nm), λ is the wavelength of the radiation used, θ is the angle of the selected peak (radians) and β is the full width of the selected peak at half maximum intensity (radians). K factor of cubic particles of 0.90 was used.

2.3 CO_2 photoreduction test

The photoactivity of the developed MWCNT@TiO_2 nanocomposites was tested in a continuous and low pressure CO_2 photoreduction system (Fig. 1) as reported in our previous work.[18,19] In the reactor system, quartz tube with the dimensions of 10mm x 200mm (OD x length) was used as a photoreactor. A digital thermocouple was inserted into the reactor to monitor the temperature. A 15W energy saving light bulb (Philips) was used as the source of visible light. Figure S1 provides the light spectrum of the energy light bulb (Electronic Supplementary Information). In addition, the entire photoreduction system was enclosed in a black box to avoid incoming or outgoing light from/to the surrounding. A thin layer of photocatalysts was coated on glass rods prior to be placed into the photoreactor.[18] Before the CO_2 photoreaction, the reactor was flushed with pure CO_2 at a flow rate of 30 mL/min for 30 min in dark. The photoreduction reaction was performed at a controlled CO_2 flow rate of 5 mL/min. Water was used as sacrificial reagent for the photoreduction reaction and was introduced through bubbling of the CO_2 gas in water before entering the photoreactor. During the CO_2 photoreduction, the product gas was collected using gas bags from time to time and the composition of the product gas was analyzed in a gas chromatography (GC) (Agilent 7890A, Hayesep Q and mol sieve column) equipped with both thermal conductivity detector (TCD) and flame ionization detector (FID) detectors. The methane formation was calculated using the following expression:

$$\text{Total methane formation} = \frac{\text{total amount of methane produced } (\mu mol)}{\text{amount of photocatalyst used } (g)} \quad \text{(Eq. 2)}$$

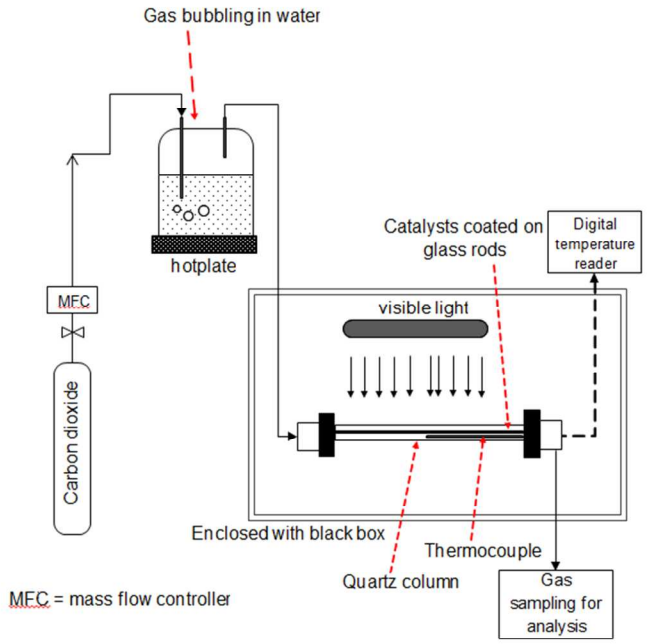

Fig. 1. Schematic of the CO_2 photoreduction system.

3. Results and Discussion

3.1 Surface morphology and structure

Fig. 2 (a-f) shows the FE-SEM images of MWCNT@TiO_2 core-shell nanocomposites prepared with various ratios of TiO_2 to MWCNTs and the acid-treated MWCNTs (Fig. 2g). The formation of thick TiO_2 layer with rigid network was observed for the samples TiOCNT1, TiOCNT2, and TiOCNT3 (Fig. 2a-c) of which the TiO_2:MWCNTs ratios of these samples were below 1:0.24. It was noted that large TiO_2 clusters were formed in these three respective samples due to excessive loading of TiO_2 that agglomerated during the synthesis process. The sample TiOCNT4, on the other hand, exhibited uniform coating of TiO_2 layer along the MWCNTs with minimum TiO_2 agglomeration observed (Fig. 2d). Non-uniform TiO_2 layer and uncoated MWCNTs were spotted from the FE-SEM images of the samples TiOCNT5 and TiOCNT6.

HRTEM analysis is an effective tool to investigate the crystallographic morphology and crystal structure of the core-shell composites through measurement of the lattice fringes. HRTEM analysis was performed on TiOCNT4, which exhibited relatively uniform TiO_2 shell layer among all the prepared samples (Fig. 2). The HRTEM analysis unveiled the morphology of the core-shell structure as a layer of TiO_2 particles wrapping the entire MWCNT surface (Fig. 3a). MWCNT-TiO_2 heterojunctions were observed indicating the existence of interaction between these two composites (Fig. 3b). The interaction between the MWCNTs and TiO_2 is an important factor for enhancing the photoactivity of the composites.[17, 20] Lattice fringe measurements confirmed that the TiO_2 nanoparticles was anatase (1 0 1) phase with the lattice spacing of 0.35nm. Meanwhile, the lattice spacing of 0.33nm was attributed to the (0 0 2) graphitic plans of the MWCNTs.

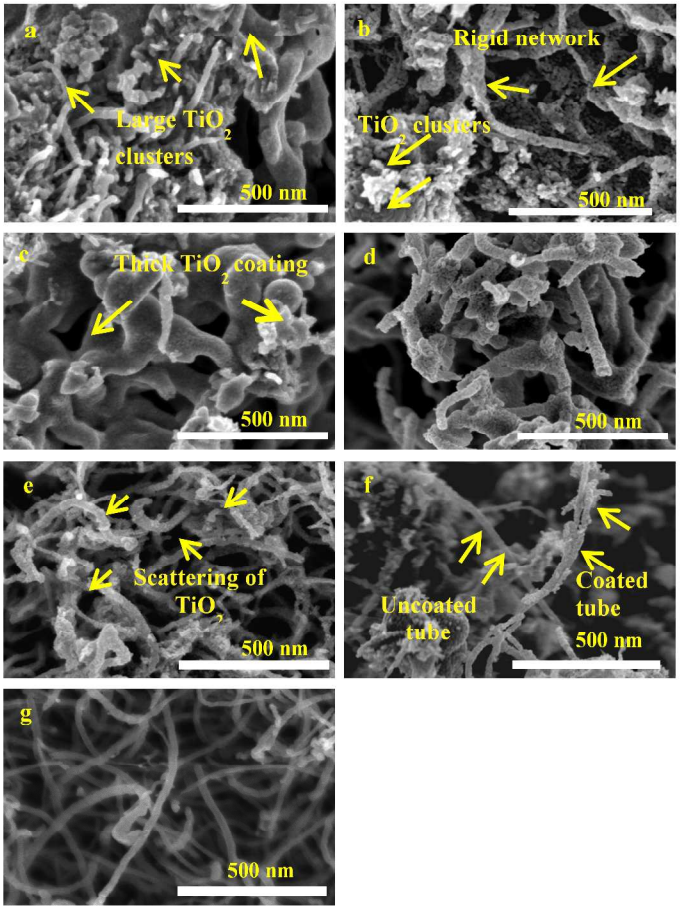

Fig. 2. FE-SEM images of the MWCNT@TiO_2 core-shell nanocomposites: (a) TiOCNT1, (b) TiOCNT2, (c) TiOCNT3, (d) TiOCNT4, (e) TiOCNT5, (f) TiOCNT6, and (g) acid-treated MWCNTs.

3.2 Optical properties

The optical properties of the core-shell nanocomposites were characterized with UV-vis spectroscopy. Fig. 4 shows the UV-vis diffuse reflectance spectra of the MWCNT@TiO_2 core-shell samples. In general, the visible light absorption of these samples was found to increase with the increase in the MWCNT loading, indicating that MWCNTs enhanced the light absorption of the entire UV-vis range. The absorption edge of the MWCNT@TiO_2 nanocomposites were found to correspond directly to the MWCNT content with the absorption edge extended to longer wavelength for increasing MWCNT loading, *i.e.* from 380nm (of TiOCNT1) to 390nm (of TiOCNT2), and 420nm (of TiOCNT3). The absorption edges of the sample TiOCNT3, TiOCNT4 and TiOCNT5 were close to the values of 420nm, 430 nm and 450nm, respectively. Among all, the sample TiOCNT6 exhibited broadest absorption shoulder with the absorption edge extended to approximately 530nm. The great improvement in the light absorption and the extended absorption edge can be attributed to the role played by the MWCNTs in the nanocomposites. The MWCNTs are believed

to act as a photosensitizer that led to the absorption of visible light.[6,8,21]

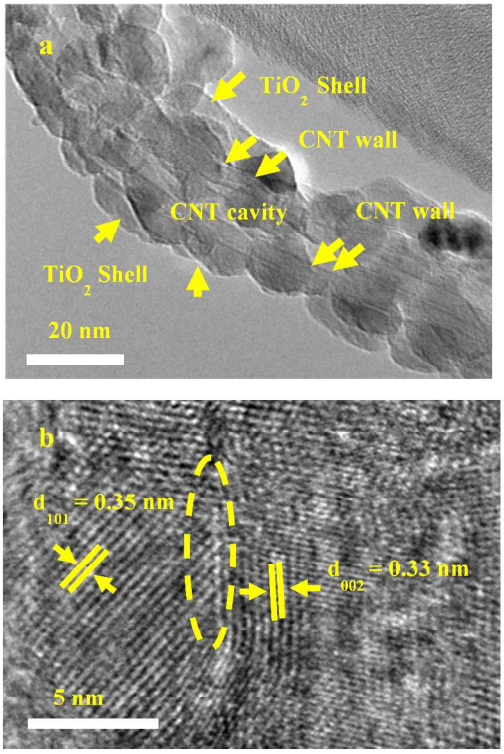

Fig. 3. HRTEM images showing (a) core-shell structure, and (b) MWCNT-TiO_2 heterojunction (dashed line) and lattice fringes.

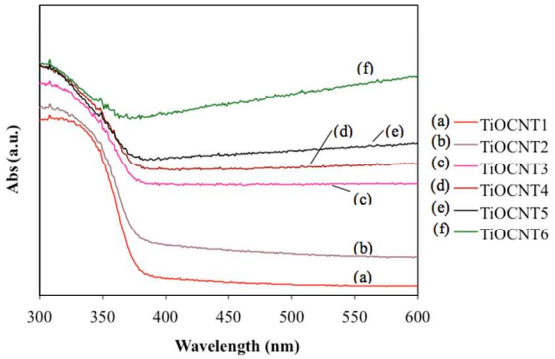

Fig. 4. Light absorption performance of the MWCNT@TiO_2 core-shell nanocomposites.

3.3 Crystal structure and surface chemistry

XRD analysis was performed to study the crystal phase information of the MWCNT@TiO_2 core-shell nanocomposites. In Fig. 5, the XRD analysis exhibited identical patterns for all of the samples, showing that the crystal structures of the TiO_2 obtained were not affected by varying the MWCNT loading. The characteristic peaks observed at 2θ = 25.2, 37.9, 48.3, 53.9, 55.0, 62.7, 68.9, 70.1, and 75.5° were correspondent to anatase phase TiO_2 with the crystal facets of (1 0 1), (0 0 4), (2 0 0), (1 0 5), (2 1 1), (2 0 4), (1 1 6), (2 2 0), and (2 1 5), respectively.[23]The crystal face (1 0 1) appeared to have the strongest intensity, thus it can be identified as the predominant crystal structure. It is also noted that no rutile phase was observed. This finding can be attributed to the relatively low calcination temperature (*i.e.* 400°C) employed in this study; wherein, the phase transformation of anatase to rutile will only happen at the temperatures of approximately 550-700°C.[6] The crystallite size of the TiO_2 nanoparticles on the shell layer was estimated using Scherrer's equation based on the predominant crystal phase (1 0 1) to be in the range of 15-23nm (summarized in Table 2).

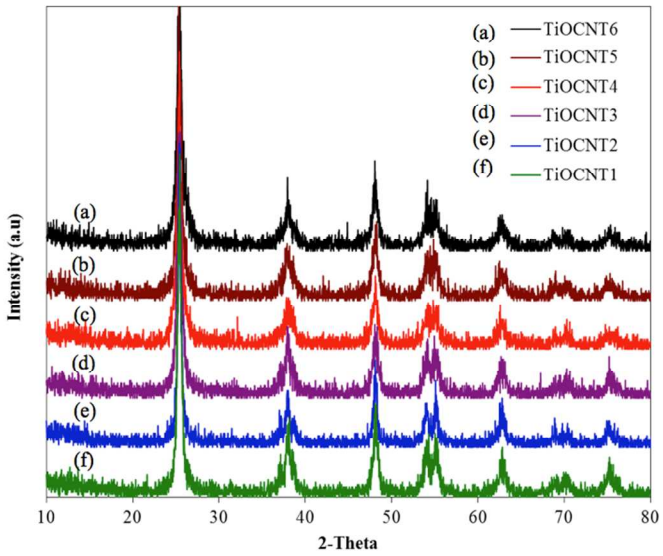

Fig. 5. XRD spectra of the developed MWCNT@TiO_2 core-shell nanocomposites.

Table 2: Summary of the crystallite sizes from XRD and (1 0 1) E_g mode position in Raman spectroscopy.

Sample name	Crystallite size in XRD (nm)	Peak position (1 0 1) in Raman (cm^{-1})
TiO_2 anatase	N/A	144.2
TiOCNT1	21	150.8
TiOCNT2	23	153.2
TiOCNT3	16	149.0
TiOCNT4	16	147.0
TiOCNT5	16	152.0
TiOCNT6	15	150.8

Fig. 6a shows the Raman spectra of the core-shell nanocomposites. In general, four characteristic peaks of anatase phase were expected from these samples, *i.e.* 150, 402, 519, and 639 cm^{-1}, of which corresponding to main E_g anatase vibration mode, B_{1g} mode, B_{1g} + A_{1g} mode, and weak E_g mode of anatase TiO_2, respectively.[9,24] These characteristic peaks were significantly observed in the Raman shifts of the samples TiOCNT1 and TiOCNT2 which were prepared by low TiO_2:MWCNTs ratios of <1:0.16. However, the characteristic peaks of B_{1g} mode, B_{1g} + A_{1g} mode, and weak E_g mode can be hardly observed in the Raman shifts for TiOCNT5 and TiOCNT6, which were prepared with TiO_2:MWCNTs ratios of greater than 1:0.24. This observation can be possibly due to the high dispersion of anatase TiO_2 nanoparticles that have led to broadening and reduced intensity of these weak peaks,

consequently causing them to be insignificant as compared to the strong characteristic peak of the main E_g vibration mode.

The Raman shifts of the main E_g vibration mode of these samples were also compared and analyzed (Fig. 6b). It was observed that the E_g vibration modes of anatase TiO_2 in the nanocomposites were blue shifted to a higher wavenumber (ranging from *ca.* 149 to 153.2cm^{-1}) from the E_g vibration mode of the commercial pure TiO_2 anatase powder (at *ca.* 144.2cm^{-1}). Furthermore, blue-shifting and red-shifting of the E_g vibration mode band position were observed for the core-shell nanocomposites developed from various MWCNT loadings. The band positions of the E_g vibration mode in these samples were summarized in Table 2. The blue/red shifting of the E_g vibration mode band position in these nanocomposites is due to the strength of the bonding between TiO_2 layer and the MWCNT core. The bonding of the TiO_2 on the MWCNTs was believed to produce different compressive stresses on the atoms of TiO_2 nanoparticles and hence resulting different vibrational wavenumbers.[25]

The ratio of the intensity of main anatase E_g mode to the intensity of graphene band (I_A/I_G) for different MWCNT loadings in the nanocomposites were estimated and compared in Fig. 6c. In general, the Raman shifts exhibited the trend with reducing intensity of E_g mode and increasing intensity of graphene band for the increase in the ratio of TiO_2:MWCNTs. Notably, the I_A/I_G was found to reduce with an increase in the MWCNT loading, indicating the abrupt reduction in the percentage of TiO_2 in the nanocomposites, especially for the samples with the TiO_2 to MWCNT ratios ranging from 1:0.04 to 1:0.24. When the TiO_2 to MWCNT ratios were further increased to 1:0.32 and 1:0.40, the I_A/I_G was found to be nearly constant. The high intensity of E_g mode (that eventually gives high I_A/I_G ratio) of TiOCNT1 and TiOCNT2 was attributed to the scattering effect from the agglomerated TiO_2 particles on the MWCNT surfaces due to highly excessive TiO_2 loading.

The changes on the surface chemistry of the MWCNTs before and after the TiO_2 coating were also investigated from the Raman shifts. Fig.7 shows the peak fitting of the *G*-bands and *D*-bands of the Raman spectra with Lorentz function for the pristine MWCNTs, acid-treated MWCNTs and MWCNT@TiO_2 core-shell composites (TiOCNT4). The peaks at 1325 and 1580cm^{-1} are attributed to the defects (*D*) and graphene (*G*) band of the MWCNTs.[9,27] Upshifting of the *G*-band by $\Delta\omega = \sim 12$ cm^{-1} was observed for the MWCNTs after acid treatment. The *G*-band of the MWCNTs was found to be downshifted by $\Delta\omega = \sim 9$ cm^{-1} after coating with the TiO_2 layer. Upshifting and downshifting of the *G*-bands can be identified as an indicator of electron transfer from the MWCNTs to the neighboring molecules and *vice versa*. It was reported that upshifting of the *G*-band occurs with the presence of electron acceptor molecules.[28] In this case, it can be attributed to the transfer of electrons from the MWCNTs to the covalent bonded (-COOH) groups on the MWCNT surface introduced during the acid treatment step. On the other hand, downshifting of the *G*-band can be attributed to the transfer of electrons from TiO_2 to MWCNTs.[28-30] This observation explains the enhancement of visible light absorption performance and extended absorption edge into visible range for the MWCNT@TiO_2 nanocomposites as compared to commercial anatase TiO_2.

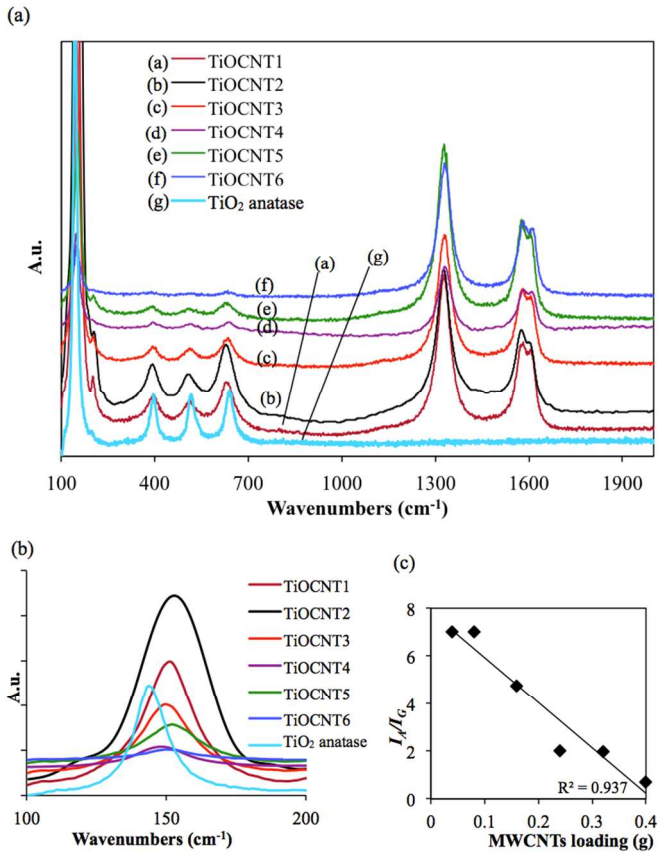

Fig. 6. (a) Raman shifts of the nanocomposites synthesized with different MWCNT loadings, (b) Raman shifts of the E_g anatase vibration mode, and (c) Plot of I_A/I_G against various MWCNT loadings.

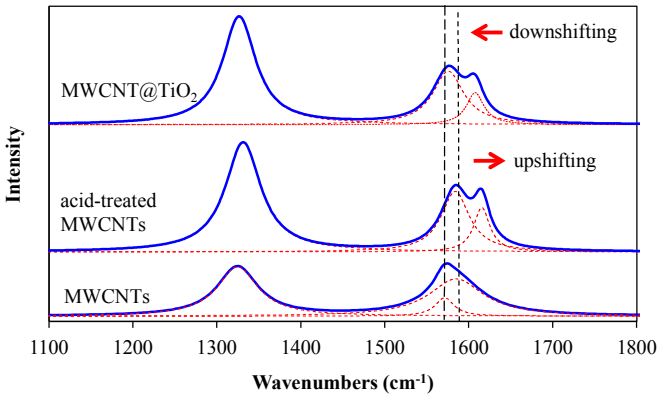

Fig. 7. Raman shifts and Lorentz fitting of *D*- and *G*-bands of the pristine MWCNTs, acid-treated MWCNTs, and MWCNT@TiO_2 core-shell nanocomposites.

3.4 PL analysis and electron charge recombination

PL analysis was used to measure the radiative recombination of the self-trapped electrons upon photoexcitation of the developed MWCNT@TiO_2. The recorded PL spectra were

shown in Fig. 8. From the PL results, one can observe that the intensity of the peak centered at *ca.* 580nm decreased with the increase in the MWCNT loading. The radiative recombination rates of the electron (e^-) - hole (h^+) can be measured from the peak intensity of the PL spectra. Referring to Fig. 8, the radiative recombination rates of these core-shell nanocomposites were significantly decreased with the increase in the MWCNT loading indicating that there is inhibition of electron charge recombination with the presence of MWCNTs. It is also believed that the MWCNTs would act as electron storage to trap part of the electrons generated from the photoexcitation of the TiO_2 shell upon irradiated with the light source as well as the "bridge" that transferred the electrons from the TiO_2 to CO_2 molecules that absorbed on the TiO_2 surface. These two phenomena led to the reduction of the electron concentration trapped in the TiO_2, eventually contributing to the inhibition of the electron-hole pair recombination.

It is believed that the electron charge transfer between MWCNTs and TiO_2 nanoparticles was taken place through the MWCNT-TiO_2 heterojunction. The sample TiOCNT6 was identified to have the highest electron charge transfer efficiency with the least electron recombination rates as divulged by the PL results. However, this sample may not be the best photocatalyst due to the fact that low electron recombination rate can also be caused by the low electron photoexcitation rate due to less TiO_2 active sites present in this sample.[7] Therefore, photocatalytic studies were carried out for all the MWCNT@TiO_2 core-shell nanocomposites to further examine their performance in CO_2 reduction.

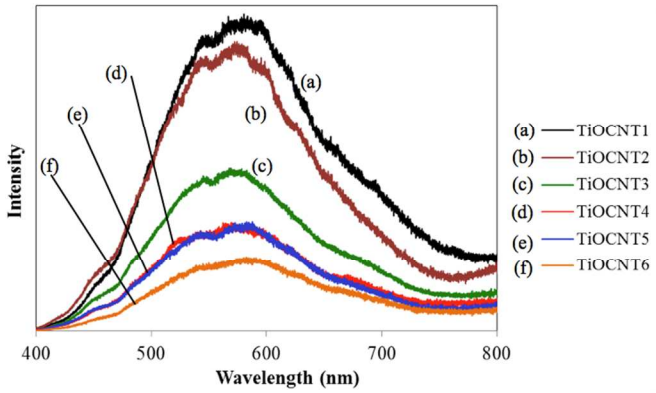

Fig. 8. PL spectra of the developed MWCNT@TiO_2 nanocomposites.

3.5 CO_2 photoreduction performance

CO_2 photoreduction was studied in a continuous, low pressure reactor system under irradiation with 15W energy saving light bulb. Fig. 9 shows the total methane formation for 8h of reaction over the core-shell samples. The total amount of methane produced was found to increase with the increase in TiO_2:MWCNTs ratio until reaching the optimum value of 1:0.24 and subsequently decreased with further increasing the MWCNT loading. The sample TiOCNT4 gave the highest methane formation of 1.10μmol/g-TiO_2 from CO_2 photoreduction; whereas, TiOCNT5 and TiOCNT6 exhibited lower methane formation as a result of less TiO_2 active sites present. Superior photoreactivity in TiOCNT4 as compared to other samples can be attributed to the uniform TiO_2 shell layer as supported by the FE-SEM image in Fig. 2(d).

During the CO_2 photoreduction reaction, MWCNT@TiO_2 nanocomposites with absorption edge extended into the visible light range could be easily photoexcited by the visible light source of low energy content, leading to electron-hole separation that generated electron (e_{cb}^-) - hole (h_{vb}^+) pairs (Eq. 3).[1,23] The electron-hole pairs generated upon the photoexcitation process was then transferred from the lattice to the surface of the TiO_2 shell.

$$TiO_2 + hv \rightarrow TiO_2(e_{cb}^-) + TiO_2(h_{vb}^+) \quad \text{(Eq. 3)}$$

The electrons and holes when contacted with CO_2 and water (sacrificial reagent) initiated the photoreduction reaction that formed OH• radicals and H^+ protons. Water received the holes (h_{vb}^+) from the surface of TiO_2 underwent the photo-oxidation, forming OH• radicals and H^+ protons (Eq. 4). The H^+ protons subsequently reduced the CO_2 molecules *via* photoreduction reaction that led to the formation of methane by consuming a total of 8 electrons for each mole of the methane produced (Eq. 5).[31-33]

$$H_2O + h_{vb}^+ \rightarrow OH\bullet + H^+ \quad E^o = +2.32\ V \quad \text{(Eq. 4)}$$

$$CO_2 + 8H^+ + 8e_{CB}^- \rightarrow CH_4 + 2H_2O \quad E^o = -0.24V \quad \text{(Eq. 5)}$$

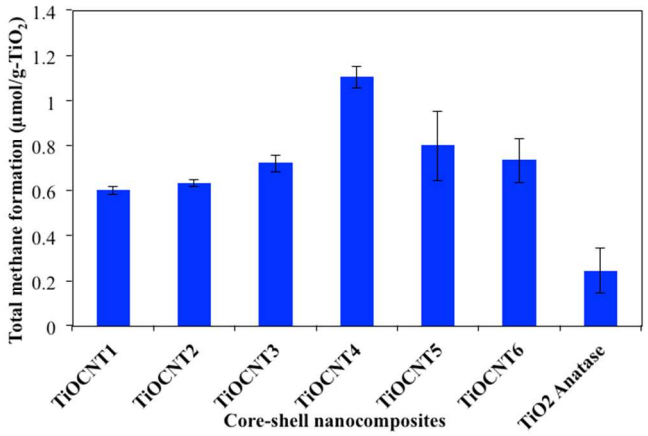

Fig. 9. Total methane formation over the core-shell nanocomposites with different MWCNT loading.

Conclusions

The developed MWCNT@TiO_2 core-shell nanocomposites exhibited promising photoactivity for CO_2 reduction. The introduction of MWCNTs has enhanced the photoactivation of TiO_2 under the visible light irradiation. The UV-vis spectra of the developed samples showed extended absorption edge into visible range with increasing MWCNT loading. On the other

hand, the radiative electron-hole photorecombination was found to decrease with the increase in the MWCNT loading as supported by the PL results. The TiO_2:MWCNTs ratio of 1:0.24 (g/g) gave the highest methane formation of 1.10μmol/g-TiO_2 despite the reaction was carried out at atmospheric temperature, pressure in a continuous system, and irradiated with a low power energy saving light bulb of 15W.

Acknowledgements

The authors would like to thank Ministry of Higher Education Malaysia (LRGS/2110226-113-00; FRGS/1/2013/TK05/MUSM/02/1) and Monash University Malaysia for the financial support given.

Notes and references

[a]Multidisciplinary Platform of Advanced Engineering, Chemical Engineering Discipline, School of Engineering, Monash University, Jalan Lagoon Selatan, 46150 Bandar Sunway, Selangor, Malaysia.
[b]Innovative Catalysis Program, Key Lab of Organic Optoelectronics & Molecular Engineering, Department of Chemistry, Tsinghua University, Beijing, 100084, China.
[c]Low Carbon Economy (LCE) Group, School of Chemical Engineering, Universiti Sains Malaysia, Engineering Campus, Seri Ampangan, 14300 Nibong Tebal, Pulau Pinang, Malaysia.
† Corresponding author. Tel.: +603-55146234; Fax: +603-55146207. E-mail address: chai.siang.piao@monash.edu (S.-P. Chai).
Electronic Supplementary Information (ESI) available: [light spectrum of the visible light source used in this work]. See DOI: 10.1039/b000000x/

1 S.S. Tan, L. Zouand E. Hu, *Catalysis Today*, 2006,**115**, 269.
2 K. Kočí, L. Obalová, L. Matějová, D. Plachá, Z. Lacný, J. Jirkovský, et al., *Applied Catalysis B: Environmental*, 2009, **89**, 494.
3 G.R. Dey, A.D. Belapurkar and K. Kishore, *Journal of Photochemistry and Photobiology A: Chemistry*, 2004, **163**, 503.
4 W. Feng, Y. Feng, Z. Wu, A. Fujii, M. Ozaki, K. Yoshino, *Journal of Physics: Condensed Matter*, 2005, **17**, 4361.
5 A. Kongkanand and P.V. Kamat, *ACS Nano*, 2007, **1**, 13.
6 N. Bouazza, M. Ouzzine, M.A. Lillo-Ródenas, D. Eder and A. Linares-Solano, *Applied Catalysis B: Environmental*, 2009, **92**, 377.
7 J. Yu, T. Ma and S. Liu, *Physical Chemistry Chemical Physics*, 2011, **13**, 3491.
8 Y. Cong, X. Li, Y. Qin, Z. Dong, G. Yuan, Z. Cui, et al., *Applied Catalysis B: Environmental*, 2011, **107**, 128.
9 Y. Yu, J.C. Yu, J.-G. Yu, Y.-C. Kwok, Y.-K. Che, J.-C. Zhao, et al. *Applied Catalysis A: General*, 2005, **289**, 186.
10 D. Eder, I.A. Kinloch and A.H. Windle, *Chemical Communications*, 2006, **0**, 1448.
11 D. Eder and A.H. Windle, *Journal of Materials Chemistry*, 2008, **18**, 2036.
12 L. Tian, L. Ye, K. Deng and L. Zan, *Journal of Solid State Chemistry*, 2011, **184**, 1465.
13 H. Wang, H.-L. Wang and W.-F. Jiang, *Chemosphere*, 2009, **75**, 1105.
14 Y. Ou, J. Lin, S. Fang and D. Liao, *Chemical Physics Letters*, 2006, **429**, 199.
15 F. Wang and K. Zhang, *Current Applied Physics*, 2012, **12**, 346.
16 W. Zhou, K. Pan, Y. Qu, F. Sun, C. Tian, Z. Ren, et al., *Chemosphere*, 2010, **81**, 555.
17 S. Qin, F. Xin, Y. Liu, X. Yin and W. Ma, *Journal of Colloid and Interface Science*, 2011, **356**, 257.
18 M.M. Gui, S.-P. Chai, B.-Q. Xu and A.R. Mohamed, *Solar Energy Materials and Solar Cells*, 2014, **122**, 183.
19 W.-J. Ong, M.M. Gui, S.-P. Chai and A.-R. Mohamed, *RSC Advances*, 2013, **3**, 4505.
20 J.A. Rodríguez-Manzo, F. Banhart, M. Terrones, H. Terrones, N. Grobert, P.M. Ajayan, et al., *Proceedings of the National Academy of Sciences*, 2009,**106**,4591.
21 M.-L. Chen, F.-J. Zhang and W.-C. Oh, *New Carbon Materials*, 2009, **24**, 159.
22 N. Sasirekha, S.J.S. Basha and K. Shanthi, *Applied Catalysis B: Environmental*, 2006, **62**, 169.
23 Q.-H. Zhang, W.-D. Han, Y.-J. Hong and J.-G. Yu, *Catalysis Today*, 2009, **148**, 335.
24 W.F. Zhang, Y.L. He, M.S. Zhang, Z. Yin and Q. Chen, *Journal of Physics D: Applied Physics*, 2000, **33**, 912.
25 C.Y. Xu, P.X. Zhang and L. Yan, *Journal of Raman Spectroscopy*, 2001, **32**, 862.
26 H.C. Choi, Y.M. Jung and S.B. Kim, *Vibrational Spectroscopy*, 2005, **37**, 33.
27 Y. Luo, Y. Heng, X. Dai, W. Chen and J. Li, *Journal of Solid State Chemistry*, 2009, **182**, 2521.
28 R. Graupner, *Journal of Raman Spectroscopy*, 2007, **38**, 673.
29 U.J. Kim, C.A. Furtado, X. Liu, G. Chen and P.C. Eklund, *Journal of the American Chemical Society*, 2005, **127**, 15437.
30 A.M. Rao, P.C. Eklund, S. Bandow, A. Thess and R.E. Smalley, *Nature*, 1997, **388**, 257.
31 C.-C. Lo, C.-H. Hung, C.-S. Yuan and J.-F. Wu,*Solar Energy Materials and Solar Cells*, 2007, **91**, 1765.
32 N.M. Dimitrijevic, B.K. Vijayan, O.G. Poluektov, T. Rajh, K.A. Gray, H. He, et al., *Journal of the American Chemical Society*, 2011, **133**, 3964.
33 Y. Li, W.-N. Wang, Z. Zhan, M.-H. Woo, C.-Y. Wu and P. Biswas, *Applied Catalysis B: Environmental*, 2010, **100**, 386.

Table of Content

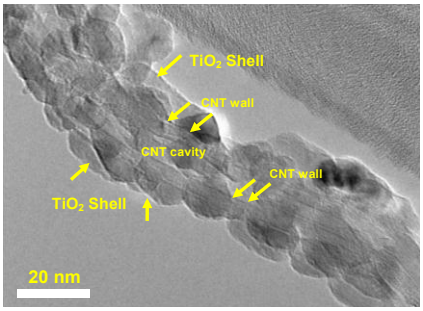

– The light absorption performance, surface chemistry and photoreactivity of the MWCNT@TiO_2 core-shell in CO_2 reduction were studied.